New Adaptation of Actuator Disc Method for Aircraft Propeller CFD Analyses

György Bicsák and Árpád Veress

Budapest University of Technology and Economics, Department of Aeronautics, Naval Architecture and Railway Vehicles
Műegyetem rkp. 3, H-1111 Budapest, Hungary
e-mail: gybicsak@vrht.bme.hu, averess@vrht.bme.hu

Abstract: The present paper is dedicated to introducing an accurate, generally applicable and minimum requirement demanding quasi steady-state CFD simulation method for investigating the effect of an aircraft propeller within the framework of the ESPOSA project. The simplest solution has been looked for in low Mach number flow regime, thus instead of direct discretization or using source terms, the Actuator Disk Method (ADM) has been applied with two different boundary condition settings: applying induced velocities or total pressure. Formerly, the Rotating Domain Model (RDM) has been validated, thus its output can be used as the reference solution. The results of the three models have been investigated both qualitatively and quantitatively. The most problematic part was the engine nacelle and propeller interaction, which has a strong influence on propeller efficiency. The investigation has shown that the ADM with total pressure boundary condition settings can provide acceptably close results to the reference RDM: within 5% amongst the investigated parameters.

Keywords: Actuator Disk Model; Schmitz method; Rotating Domain Model; Reynolds-Averaged Navier-Stokes Simulation; propeller-body interaction

1   Introduction

One of the most challenging problems nowadays is satisfying the continuing demands of increasing air traffic and introducing breakthrough innovations, leading technologies and green, sustainable solutions. These goals require fast and accurate solutions, for which purpose several outstanding R&D (Research and Development) projects are in progress [1], [2], [3], [4] and [5]. The design and optimization [6] of air-flows and structures in relation to jet engines, turboprops, helicopter rotors [7] and other turbo-machinery related configurations is a complex and cost demanding process. Especially for having accurate performances [8] and aerodynamic parameters, while expecting the application of proper material properties to maintain structural integrity [9]. The design and analyses in a spatially distributed manner are becoming more highlighted today

due to its effectivity [10], not only transportation such as aviation, ships and marine propulsion [11], [12] but also in the other segments of the industry. Novel design, sizing and calculation technologies are becoming available in both light and very light jet aircraft according to new trends [13].

In this paper, an accurate and fast CFD (Computational Fluid Dynamics) application is introduced within the framework of the ESPOSA (Efficient Systems and Propulsion for Small Aircraft) project [14]. The project itself is based on cost-efficient solutions, which enable and ensure access to development methods for smaller companies to design their own small aircraft type, while following the most up-to-date safety laws, regulations and recent international project goals, such as, the Clean Sky Project, and still reducing the overall cost demands. The BME (Budapest University of Technology and Economics) Department of Aeronautics, Naval Architecture and Railway Vehicles participates in the ESPOSA project and has the task of improving design specifications of the engine intake channel and nacelle of a newly developed tractor turboprop aircraft with numerical methods. The induced velocity distribution of the propeller has been determined by Schmitz's method and has been used in the flow modelling software as boundary conditions.

Beside the developments and/or applications of different CFD methods in the wide range of engineering coverage - as it is observable today in the state of the publications at different length scales: [4], [7], [15] - these approaches are highly capable also of investigating the airflow around rotor blades – propeller aerodynamics [16], or even the load distribution on the rotors [17]. The goal of this investigation is to establish a RANS (Reynolds Averaged Navier-Stokes Simulations) based (due to its reduced computational demand compared to Large Eddy Simulations) cost effective ADM method, which is capable of providing general, fast and accurate results in the pre- and serial-development phases of a new product by replacing several experimental results. The actuator disk method originates from the pioneering work of Rankine [18] and Froude [19], which still constitutes, in conjunction with the blade element theory, the most used analysis and design tool for aircraft propellers and wind turbines. A landmark review on this matter is presented by Glauert [20]. Wu [21] gives the exact and implicit solution of the flow through a generalized actuator disk. Conway [22] introduced explicitly Wu's solution through a semi-analytical procedure, which was later extended by Bontempo and Manna [23] [24] to ducted rotors with or without an axisymmetric hub of general shape. In order to reduce the computational cost related to the simulation of a geometrically resolved rotor, an actuator disk is often introduced in CFD codes.

The actuator disc method is already a well-determined concept, several papers and articles have been published to present different applications. One of the most significant fields is the modelling of airflow adjacent to wind turbine propellers, as represented by the following papers: an improved ADM was developed by Costa Gomes, Palma and Silva Lopes [25]; the ADM was applied by porous cells for wake modelling purposes in the publication of Gravdahl, Crasto, Castellani and Piccioni [26].

Regarding the aeronautical applications, Yu, Samant and Rubbert [27] developed an Euler solver for predicting flow field for propfan configuration using the actuator disc method. Although the theory behind the specification of the downstream disc surface boundary conditions is based on the total pressure, total temperature and flow angles, the method provided is rather code-dependent; it is difficult to generalize due to the extrapolation of the velocity from the computational domain. In other counterparts of the aerospace applications it is still a particularly important field of investigation, especially for helicopter, hover or tilt-rotor applications, as the following relevant examples show: LeChuiton [28], Visingardi, Khier and Decours [29], Conlisk [30], Farrokhfal and Pishevar [31], or Wald [29]. Lenfers [32] performed research in the design process on turboprop engine rotor, and Jeromin, Bentamy and Schaffarczyk [17] completed a rotor analysis in a wind tunnel.

As Coton, Marshall, Galbraith and Green have discussed the interaction of the rotor and an object nearby has been a subject of discussion for almost 30 years [33], of which most studies focus on the solution. Indeed, within the frame of the present paper, the novel actuator disk model has been developed with such boundary conditions that make it possible to investigate the effect of a nearby object on the propeller efficiency in general. The need for such a solution is required, as the actuator disk model generates a uniform induced velocity at the rotor disk [22], which is a constant boundary condition regardless of the environmental objects and distributions. Because of this, it is also worth mentioning that there is a different way in which the source terms are applied to the actuator disc surface imparting impulse and energy to the fluid, as Le Chuiton published it [28]. However, the generalization and the control of this approach with respect to the blockage in the flow field, for example, is not always possible and rather complicated comparing that with the presently applied procedure.

2   Theoretical Fundamentals

The governing equations in the present CFD simulations are the Navier-Stokes equations (together with mass and energy conservation laws) due to the Knudsen number being below 0.01 within the framework of the ANSYS CFX. The considered system of the nonlinear partial differential equation in their conservative form is valid: for both laminar and turbulent flows, for compressible one component ideal gas in a steady state inertial system, for a homogeneous isotropic material, in which the frictional processes are taken into account together with no potential field, such as gravity or magnetic forces, for example except for the rotating domain, where the inertial forces and their effects are considered and with the assumption of no sources or sinks are available. In order to avoid the uncertainty coming from the turbulent fluctuation while preserving the description of its effect in momentum transfer and from an energetics point of view, the corresponding parameters are averaged by Reynolds. The governing equations are the mass, momentum and total energy equations, in order [35]:

$$\frac{\partial \rho}{\partial t} + \nabla \cdot (\rho \boldsymbol{U}) = 0 \tag{1}$$

$$\frac{\partial (\rho \boldsymbol{U})}{\partial t} + \nabla \cdot (\rho \boldsymbol{U} \otimes \boldsymbol{U}) + \nabla p - \nabla \cdot \tau = \boldsymbol{S_M} \tag{2}$$

$$\frac{\partial (\rho h_{tot})}{\partial t} - \frac{\partial p}{\partial t} + \nabla \cdot (\rho \boldsymbol{U} h_{tot}) - \nabla \cdot (\lambda \nabla T) - \nabla \cdot (\boldsymbol{U} \cdot \tau) = \boldsymbol{U} \cdot \boldsymbol{S_M} + \boldsymbol{S_E} \tag{3}$$

where ρ stands for density, $\boldsymbol{U}$ is the velocity vector, p marks the pressure, τ is the stress tensor, h_{tot} is the total enthalpy, λ represents the thermal conductivity finally $\boldsymbol{S_M}$ and $\boldsymbol{S_E}$ are source terms. Following the Boussinesq approximation for modelling the components of Reynolds stress tensor, SST (Shear Stress Transport) turbulence model has been used in the all investigated cases. It combines the advantages of the k-ω and k-ε models. Blending functions control the usage of a k-ω formulation in the inner parts of the boundary layer makes the model directly usable all the way down to the wall through the viscous sub-layer. The SST formulation switches to the k-ε behaviour by the blending function in the free-stream and thereby avoids the common k-ω problem that the model is too sensitive to the free-stream value of the turbulence variables (in particular ω). The further distinction of the SST turbulence model is the modified turbulence eddy-viscosity function. The purpose is to improve the accuracy of prediction of flows with strong adverse pressure gradients and pressure-induced boundary layer separation. The modification accounts for the transport of the turbulent shear stress, which is based on Bradshaw's assumption that the principal shear stress is proportional to the turbulent kinetic energy [34].

Rotating Domain Model

One of the applied models is the RDM. The base of this approach is that the propeller blades with the hub and the adjacent fluid domain rotate with the angular velocity of the turboprop. This model is basically considered as the most accurate one, but to simulate the wall boundary effect correctly, a fine mesh is necessary, which significantly increases the computational time and performance demand.

Because the fluid also rotates together with the rotating blades with a constant angular velocity, additional components are required in the governing equations. The centrifugal force and Coriolis force's effects are included in the momentum equation with the following sources [35]:

$$S_{M,rot} = S_{Cor} + S_{cfg} = -2\rho\Omega \times U - \rho\Omega \times (\Omega \times r) \tag{4}$$

In the energy equation, the advection of the enthalpy has to be replaced by the advection of rothalpy (I) in the following form [35]:

$$I = h + \frac{1}{2}U^2 - \frac{1}{2}\Omega^2 r^2 \tag{5}$$

Schmitz Method for the Actuator Disk Model

The output of the present calculation is the required power of the propeller and the distribution of the induced velocities in the radius. The condition of the calculation is that the given power be equal to the calculated power at the belonging blade setting. The results of the present propeller analyses are used for the boundary conditions of the CFD analysis in the ADM models.

The swirling effect of the propeller is simulated by adopting the actuator disc model based on Schmitz method. This model deals with the aerodynamic forces created by the airflow around the propeller blade elements. The calculation uses the combined Blade Element and Momentum Theory [30]. The mathematical model has the following input data:

- air density and temperature (depends on the flight altitude, based on International Standard Atmosphere data; $\rho = 0.9048 \ kg/m^3$, $T = 268.4 \ K$);
- free stream (flight) velocity of the aircraft (112 m/s);
- diameter and RPM (Rotation Per Minute) of the propeller (2.08 m and 1950 RPM);
- blade number (4 pcs.), blade profile, chord, and the relative blade thickness at 75 % of the blade length;
- c_L^α and c_D^α (angle of attack dependent lift and drag coefficients) curves of the profile NACA 4412.

Although the density here is stated as a constant value, this assumption is valid only to determine the induced velocity components. During the CFD simulation cases the density can be changed. The aerodynamic forces, velocity triangles and notations are illustrated in Figure 1. The induced velocity in the "lift" direction is marked as v_L, while the induced velocity in the "drag" direction is marked as u_D.
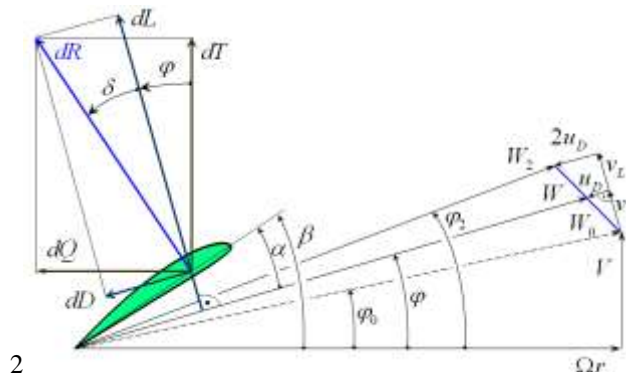

Figure 1

Velocity and force components at a blade element [36] //note: modified figure from cited source

The relative velocity of the profile (W) is expressed by the relative base velocity (W_0) constructed by peripheral (Ωr), flight speed (V) and induced velocity u_D [36]:

$$W = W_0 \cos(\varphi - \varphi_0) - u_D \tag{6}$$

Based on Figure 1 notations, the elementary drag force (dD) and lift force (dL) can be determined by momentum theory from which the first and second connection equations, between the blade-element and momentum theory, can be expressed by the two sides of the right equalities [36]:

$$dD = d\dot{m}(2u_D) = \rho(2\pi r dr)W \sin\varphi \,(2u_D) = Bc_D \frac{\rho}{2}W^2 c \, dr \tag{7}$$

$$dL = d\dot{m}(2u_L) = \rho(2\pi r dr)W \sin\varphi \,(2v_L) = Bc_L \frac{\rho}{2}W^2 c \, dr \tag{8}$$

In equation (7) and (8) c is the chord distribution of the rotor, and actually is the function of the distance from the rotation axis ($c=c(r)$), B is the number of blades, dr is the elementary radius, r is the radius, c_L and c_D are the lift and drag coefficients respectively. Based on the connection equation (7) and velocity triangle in Figure 1, the induced velocity components in the direction of drag and lift forces are the followings [36]:

$$u_D = \frac{B\,c}{8\pi r}\frac{c_D}{\sin\varphi}W \text{ and } v_L = W_0 \sin(\varphi - \varphi_0), \tag{9}$$

By combining the first equation in (9) and equation (6), the relative base velocity is next [36]:

$$W_0 = \frac{W}{\cos(\varphi - \varphi_0)}\frac{\frac{8\pi r}{Bc}\sin\varphi + c_D}{\frac{8\pi r}{Bc}\sin\varphi} \tag{10}$$

By substituting equation (10) to equation (8) (with replacing v_L by (9)) one gets:

$$2\pi r \sin\varphi \left[2\frac{W}{\cos(\varphi - \varphi_0)}\frac{\frac{8\pi r}{Bc}\sin\varphi + c_D}{\frac{8\pi r}{Bc}\sin\varphi}\sin(\varphi - \varphi_0)\right] = \frac{W}{2}Bcc_L \tag{11}$$

After simplifying equation (11) it can be written:

$$cc_L - \left[\frac{8\pi r}{B}\sin\varphi + cc_D\right]\tan(\varphi - \varphi_0) = c_L - \left[\frac{4}{\sigma}\sin\varphi + c_D\right]\tan(\varphi - \varphi_0) = 0, \tag{12}$$

which is the base equation of the calculation (propeller solidity: $\sigma = Bc/(2\pi r)$). If the solutions (φ, c_L, c_D) were substituted in (12) the expression becomes 0. But if different values are used than the solutions, there would be a non-zero residuum $\Re$ as it is found below:

$$c_L - \left[\frac{4}{\sigma}\sin\varphi + c_D\right]\tan(\varphi - \varphi_0) = \Re \tag{13}$$

(13) is a non-linear equation for φ, c_L, c_D, which are dependent variables of each other. Thus, the numerical calculation can be done by using Newton iteration to find the value φ (and then c_L and c_D can be calculated by $c_L - \varphi$ and $c_D - \varphi$ plots) [36]:

$$\varphi_{NEW} = \varphi_{OLD} - \frac{\Re}{\frac{\partial\Re}{\partial\varphi}} \tag{14}$$

where the derivative of the residuum $\Re$ is [36]:

$$\frac{\partial \Re}{\partial \varphi} = \frac{\partial c_L}{\partial \varphi} - \left[\frac{4}{\sigma}\cos\varphi + \frac{\partial c_D}{\partial \varphi}\right]\tan(\varphi - \varphi_0) - \left[\frac{4}{\sigma}\sin\varphi + c_D\right][1 + \tan(\varphi - \varphi_0)^2] \quad (15)$$

In this work, the tip-loss correction is neglected. Although at the blade tip the induced velocities are 0 in reality, the partner institute hasn't applied it in the project [37], so in this way, the results were more comparable in the final report. Of course, one of the improvement possibilities is to incorporate the blade tip loss. The induced velocities in axial and tangential direction can be calculated if v_L and u_D are determined [36]:

$$v = v_L \cos\varphi - u_D \sin\varphi \quad \text{and} \quad u = v_L \sin\varphi + u_D \cos\varphi \qquad (16)$$

In order to use the induced velocities as actual boundary conditions, they have to be multiplied by two and the flight speed is added to the axial induced speed. Furthermore, the static temperature and incoming flow direction are specified also.

This work is dedicated to highlighting the differences between two boundary conditions, and compares the results to the base rotating domain provided data. The computed v and u are used in ADMv1 model, while ADMv2 requires a slight additional calculation: the density is supposed to be constant within an infinitesimal volume of the fluid that moves with the flow velocity, so the flow is supposed to be incompressible (M_{local}=0.34-0.37). Hence, the absolute total pressure distribution along the radius is calculated from the induced speeds and flight velocity (V) with the following equation:

$$p_{total} = p + \frac{\rho}{2} \cdot [(2v + V)^2 + (2u)^2] \qquad (17)$$

The static temperature, pressure and density at flight altitude are determined by ISA (International Standard Atmosphere) [37]. As later described (see the description of rotor), the ADMv2 applies total pressure inlet values with constraint airflow direction, instead of defining the velocity vector in the rotor sweeping surface.

3 Introduction of the goals and Analyzed Aircraft Configuration

The goal of the ESPOSA project is to provide designing methods for small aircraft manufacturers by implementing new approaches or coupling already well-established methods. Since this work has been performed during the project, no experimental data were available for the behaviour of the configuration, but wind-tunnel tests have provided data for the propeller itself. Since the rotating domain had been validated earlier as a method that can provide results within 3%, this approach has been used later as a baseline model. The actuator disc method provided induced velocities were applied as boundary conditions (ADMv1) and

the relative total pressure has been set on the actuator disc surface (ADMv2). The point is to introduce that ADMv1 cannot handle the existence of adjacent objects: setting velocities results in an axisymmetric boundary condition, although the presence of wing, nacelle and engine intake influence the velocities, torque induced by the propeller.

The investigated aircraft is a high-wing, twin engine, turboprop, multi-purpose aircraft for transportation of passengers and/or cargo to be designed and produced by a partner company [40]. The nose landing gear of the aircraft is retractable; tail unit is T-shaped. Nine passengers can be transported in the unpressurized cabin with two crew members. Type AVIA tractor propellers are installed on the engines. The propellers have four blades, made from aluminium alloy and can be hydraulically actuated with single acting regulation of constant rotational speed, feathering and reversing with possibility of rotating speed and phase synchronization. The propeller blades are set to low pitch by pressurized engine oil, to the high-pitch by a spring and counter-balances on the blades. The propeller is equipped with an electrical de-icing system [41].

Geometry

The 3-dimensional CAD (Computer Aided Design) model of the analysed configuration has been provided by a partner institute [37]. In order to reduce the computation power requirements only one symmetric part of the aircraft was investigated without the fuselage. Downstream of the rotor, at the lower section of the nacelle, is the air duct inlet which is equipped with a particle and ice separator device. The separated particles are drawn through the sidewall duct outlets overboard. Upstream of the gas turbine section there is a static inlet guide vane air intake device, and downstream of the gas turbine the exhaust pipe, where the hot gas leaves the engine. At the bottom of the nacelle a cross-flow, oil-to-air type heat exchanger cools down the engine oil, which uses ambient ram airflow.

Even with this reduced geometry, the complexity of the CAD model was still too high, so some additional parts have been neglected or simplified. The rotors for the RDM and ADM have been handled in two different ways (see Figure 2):

- for the RDM all four rotor blades have been kept and a cylinder was applied around them,
- for the ADM v1 the same cylinder has been built up, but inside the cylinder everything (blades, nose cone) has been removed,
- for ADM v2 the former model has been modified: the plane surfaces of the cylinder have been divided into 10 annuli, where the boundary conditions are set.
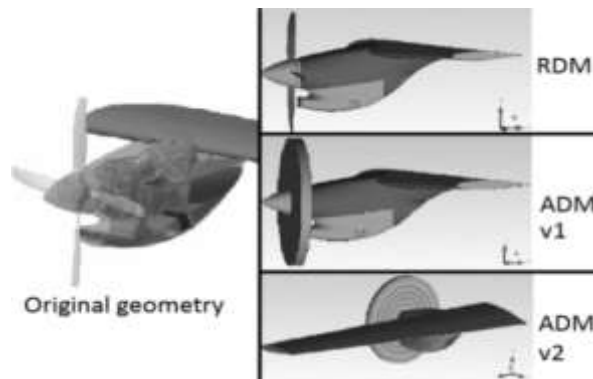
Figure 2

The original geometry [40] and simplified models for the three models *//note: original geometry is adapted from the cited source*

In order to minimise the time demand and complexity of the discretization process, the mesh has been built up using tetrahedron elements. Three-dimensional volume meshes with boundary layer subdivisions have been generated for the all domains of all versions to be investigated. Regarding the flow parameters with high gradients, local mesh refinement was applied and inflation layers provided the necessarily low $y+$ values, to be below 300 depends on the Reynolds number [35]. The global number of elements for RDM was 19,065,034, for ADM v1 and ADM v2 13,428,609.

Material Properties, Physical Settings and Boundary Conditions

The solution of the non-linear partial differential equations in a discretised form requires additional definitions. The material of the flow domains was air as an ideal gas (*γ = 1.4* and *R = 287.058 J/(kg K)*). The reference pressure of the domains has been calculated by the cruise altitude of the aircraft (3048 m) and ISA (International Standard Atmosphere) and set to 69682 Pa [14]. The effect of gravity is negligible in this case, but the viscous work term must be considered within the total energy model during modelling the heat transfer. Since the scaling varies in wide range Shear Stress Transport (SST) turbulence model is recommended for turbulence closure and 5% inlet turbulent intensity has been applied in each case [35].

Main flow

The main airflow contains the bounding volume of the flow field, the shape of the wing, engine nacelle, nosecone, oil cooler, its intake and outlet and the cylindrical surfaces, which includes the rotor and the engine exhaust surface represents the hot exhaust gas inlet into the main airflow. The main flow boundary condition settings are illustrated in Figure 3. 112 m/s cruise speed of the aircraft with 268.4 K static temperature has been set as an inlet boundary condition. 0 Pa relative pressure has been imposed on the outlet surface. Symmetry boundary condition

has been applied to the inner boundary surface, which makes possible to simplify the model: this boundary condition essentially acts as a frictionless wall. On the top, side face and bottom of the flow field "opening" boundary condition has been set with entrainment mass and momentum option and 0 Pa opening pressure [29]. This approach allows undisturbed inflow and outflow depending on the total pressure of the fluid in the computational domain and at the boundary. The engine exhaust surface has been represented to simulate the hot exhaust gas inlet into the main airflow. The mass flow of this inlet has been set equal to the engine intake outlet air and the fuel mass flow rate: 1.9759 kg/s and the static temperature of the inflowing fluid has been set to 853.3 K, based on the manufacturer's data [40].
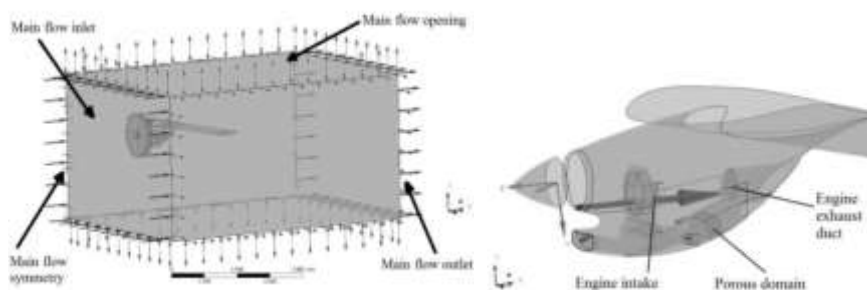

Figure 3

Boundary conditions on the main airflow domain

Heat Exchanger and Air Intake Duct

A local pressure drop is caused by the blockage of the heat exchanger in the main airflow; thus, a local low-pressure zone is formed downstream of the oil cooler heat exchanger for which purpose porous domain was used with the same volume as the heat exchanger. The pressure drop curve in the function of the normal volume flow rate has been provided by the manufacturer and has been used to determine the input parameters for the porous domain, as resistance and loss coefficient and volume porosity [40]. Indeed, the necessary calculations have been made analogically and iteratively. The scope of this paper is to introduce the settings of the rotor boundary conditions and compare the results. Thus, the calculation method is not detailed.

The role of the air duct is to collect air and forward it to the engine compressor unit with the lowest possible pressure drop, flow uniformity; and if icy conditions occur, or it is raining, separate the ice (or simply dust) particles and water droplets from the airflow to protect the compressor stage and the further part of the engine. During the investigation process of ESPOSA project, the air duct optimisation was also the scope. Hence, a separate fluid domain has been created only for the air duct in order to determine the necessary parameters – boundary conditions for the individual simulations. A general fluid to fluid interference connection has been used between the air duct separator part and main airflow. At the outlet section of the air duct (inlet of the compressor), the air demands of the engine has been imposed as a constant mass flow rate with 1.9398 kg/s.

Rotor

1.   The configuration of the RDM is the most simple: the same fluid model has to be applied, as in the case of the main flow or for the air duct domain, but a coordinate system is in the rotational axis of the rotor, around which it constantly rotates with 1950 1/min. The rotation caused rothalpy-increment generates the thrust and torque by achieving pressure rise. Since the similar model has already been validated, it is considered to be the baseline model.

2.   In the ADMv1 version, the induced velocities are calculated in the function of the distance from the rotational axis based on the propeller characteristics given in Figure 4. The continuous and dotted lines represent the axial and tangential induced velocities from the axis of rotation moving outwards along the blades. Through the front surface of the cylinder the airflow can leave the domain and across the rear surface the fluid enters. The same amount of mass flow rate is defined at the upstream surface of the disc and at the exit of the propeller plane for mass conservation, which is the same at ADM2 version too. In the inlet surface the velocity vectors and static temperature (268.4 K) boundary conditions represent the effect of the propeller. The cylindrical surface close to the tip section of the imagined blades has been set as a free slip wall, assuming that there is no airflow across this boundary.

3.   In the ADMv2 version, total pressure values were set on the inlet boundary surface in the function of the radius, constructed from the static far field pressure and dynamic pressure, which is calculated by the ambient density and local velocity vector determined at ADMv1 model. In essence, if there was an object downstream of the actuator disc, the RANS solver would create the corresponding flow field, compatible with those conditions. In our particular case to reduce computational demands, the plane surfaces have been divided into 10 annular sections, and the average total pressure has been calculated for each annulus with Simpson's method. The relative total pressure values in each section are represented by the column chart in Figure 4.
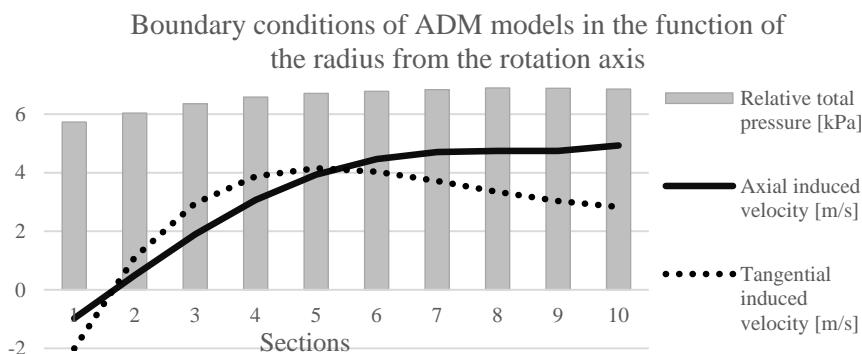
Boundary conditions of ADM models in the function of the radius from the rotation axis

Figure 4

Components of the boundary conditions of ADM models in the function of the applied sections moving from the rotational axis outwards

Solver Properties

The model has been treated as a quasi-steady-state simulation since the interest is the flow parameters and the comparison between the investigated versions during cruise phase, when the flow conditions are assumed to be constant over the time. High-resolution advection scheme has been used, just like the turbulence numeric option. The target iteration number was 1000 for the first approach, but the actual in the RDM simulation was not enough for the residuum to converge. Finally, a four times higher iteration number was needed. The ADM models' imbalances reached $2*10^{-6}$ values sooner, thus the simulation cases can be stated to be converged. The auto timescale has been applied, and the residuum target for RMS (Root Mean Square) values was 10^{-7}.

The goal of the present research was to provide a method, which is achievable with reduced computation capacities, and not necessarily require HPC (High-Performance Computing) solutions to handle the problem. Thus, the three simulations have been executed on the same computer, which is equipped with Intel® Core™ i7-3770 CPU and 8 GB RAM.

Results and Evaluation

The RDM model finally required four times more iteration number to reach the convergence criteria – in comparison with the versions of ADM – and this process took $1.3074*10^6$ CPU wall clock seconds. The ADMv1 has reached the criteria after approx. 100 iteration steps, but in order to eliminate any perturbation in the numeric solver algorithm, the computation duration has been expanded untill 600 iteration steps, which required $1.2786*10^5$ CPU seconds. In the case of ADMv2 the proceeding was the same, converged early, but the running has been extended to 600 iteration steps and lasted for $6.6713*10^4$ CPU seconds.

It is clear that the ADM approaches needs less than 10% CPU time of the RDM. This is caused by the significantly higher mesh number, but also by the longer time demand of the different residuals to drop below the convergence limit since the interface between the rotating and stationary domains causes additional disturbances in the algebraic equations. In number, it was proven that the ADMv1 has converged in 9.78% of the RDM time demand, and ADMv2 has completed in 5.1% of the RDM CPU wall clock time, so if the accuracy of the results is acceptable, the time-factor would be a serious pro for the ADM methods.

One key indicator of the results' quality and plausibility is the $y+$ number. In terms of the recent requirements, for a simulation with the given length scales and Reynolds number, the $y+$ value is maximised in 300. In the simulations, the maximum $y+$ number was 179.3 on the nacelle assembly. Meanwhile, in the case of RDM on the rotor blades, the highest $y+$ value was 107.4. Certainly, mesh sensitivity analysis was completed earlier, but in the framework of this paper, only the already checked mesh has been used. To reach the convergence criteria was no problem for the ADM simulations, generally, within 100 iteration steps the residuals dropped below 10^{-6}, and the imbalances below 1%. The RDM run on the other hand required 3500 iteration steps to achieve the same convergence.

Generally, the airflow pattern corresponds to the expectations. Upstream of the nose cone, where the airflow is decelerated, there is an increased static pressure zone. Downstream of the rotor blade sweep surface the total pressure is increased and kinetic energy has been added to the fluid by the propeller, as it is illustrated in Figure 5 bottom row. It is also obvious that there is a higher-pressure zone upstream of the air duct highlighted by the absolute static pressure distribution (middle row).
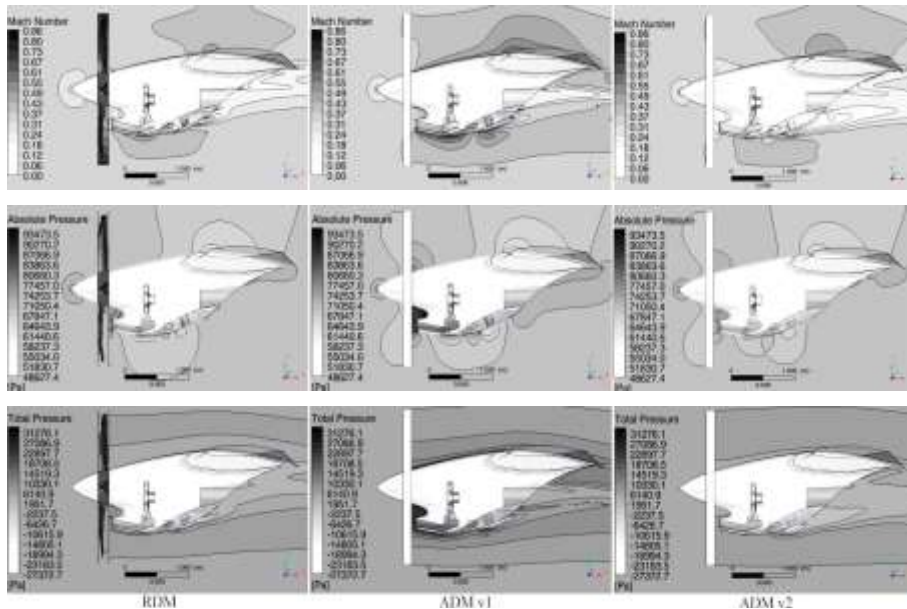

Figure 5

Representation of different parameters illustrated on the vertical mid-section plane of the engine nacelle

The compressor has a constant mass flow rate, thus the unnecessary air quantity escapes, and passes along the nacelle's side, and this blockage effect, together with the engine nacelle, also influences the velocity field downstream of the propeller blades. Basically, this phenomenon represents the problem of the ADMv1. In reality because of the discussed effect, the incoming velocities are less and deviate in particular zones due to the proximity of engine nacelle and the propellers' efficiency slightly drops. In the boundary conditions of the ADMv1 model, the velocity vectors were defined according to the calculated data and are introduced in Figure 4. These velocities are constraints, so the velocity distribution will not change downstream of the propeller. The simulation can reach this condition by increasing the local absolute total pressure at the boundary, which has produced also higher static pressure values. This phenomenon produces 10-15% higher pressure values. It cannot be observed in the other two cases. It can be also concluded that Mach number, relative static and relative total pressure

distribution pattern show similarities in the case of RDM and ADMv2 model according to Figure 5.

The different results are investigated in the function of dimensionless distance from the rotational axis. Six lines have been created downstream of the rotor, see the right upper corner of Figure 6. Both the Mach number distribution and total pressure distributions are averaged over the lines 1, 2, 3 and 4, 5, 6, which mark the significant differences caused by the different boundary condition setting between ADMv1 and ADMv2. Closer to the rotational axis, the interaction between the fluid flow and engine nacelle strongly influences the flow pattern.

In this particular area, the nacelle decreases the efficiency of the rotors, according to that the induced velocities decrease. This effect has been correctly handled by the RDM and ADMv2, but ADMv1 treats the velocities as constraints, hence the Mach number distribution (Figure 6 left upper corner) shows a significant overestimation closer to the propeller blades. The higher induced velocities come with higher local pressure values, thus the total pressure distribution has also similar pattern and confirms the better assumption of ADMv2 boundary conditions.

The total pressure distribution through the propeller/actuator disk also confirms the accuracy of ADMv2: while the average relative error between RDM and ADMv1 is 23.4%, ADMv2 reduced this error to only 3.9%, see Figure 7.
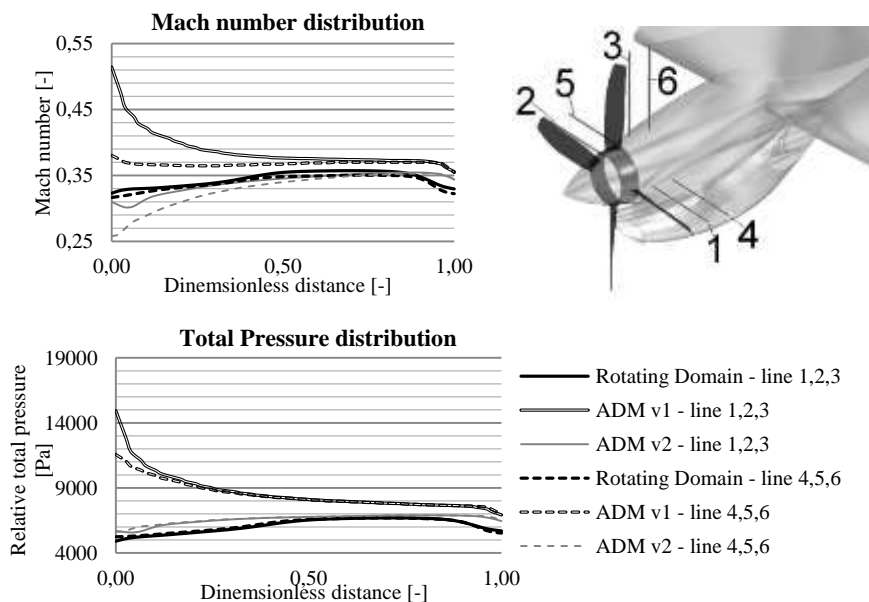

Figure 6

Lines from 1-6 downstream of the propeller sweep surface for parameter investigation (top right) and exported averaged parameters along the specified lines (top left and bottom)

The overestimated total pressure, caused by the used boundary condition treatment of the software, can be observed even better by considering the pressure distribution on the engine nacelle, see Figure 8. This comparison clearly shows that ADMv1 has computed too high-pressure values, in fact, based on Figure 5, it is higher than it is actually possible a maximum of 32% .The maximum total pressure can be calculated in the function of maximum induced and flight speeds at the downstream of the propeller plan is the following: $p_{total} = p + \frac{\rho}{2} \cdot$

$[(2v + V)^2 + (2u)^2] = 69682\ Pa + \frac{0.9048 \frac{kg}{m^3}}{2} \cdot \left[\left(2 \cdot 4.7 \frac{m}{s} + 112 \frac{m}{s} \right)^2 + \right.$

$\left. \left(2 \cdot 3.71 \frac{m}{s} \right)^2 \right] = 76374.4$ Pa. At the same time, neither of the distributions are symmetrical, the tangential components of the induced velocities create an asymmetric pattern. The engine nacelle downstream of the rotor also influences the parameters along the rotor's sweep surface by decreasing the induced velocities. This phenomenon can be observed in the case of RDM and ADMv2 cases, which is a remarkable achievement since the boundary conditions of the Actuator Disk Models are defined axis-symmetrically (considering both the velocity and pressure components), but while ADMv1 keeps the velocity distribution unchanged. ADMv2 is more flexible and can modify the velocity vector distribution, while maintaining the total pressure distribution on the demanded level.

The engine intake duct ensures a constant air-consumption, thus propeller-delivered airflow goes through the intake duct inlet. This process decreases the local absolute pressure in that particular zone. This pressure distribution, can be useful in the sizing process of the engine nacelle, to calculate the surface loads, like Renaud, O'Brien, Smith and Potsdam did it [41].
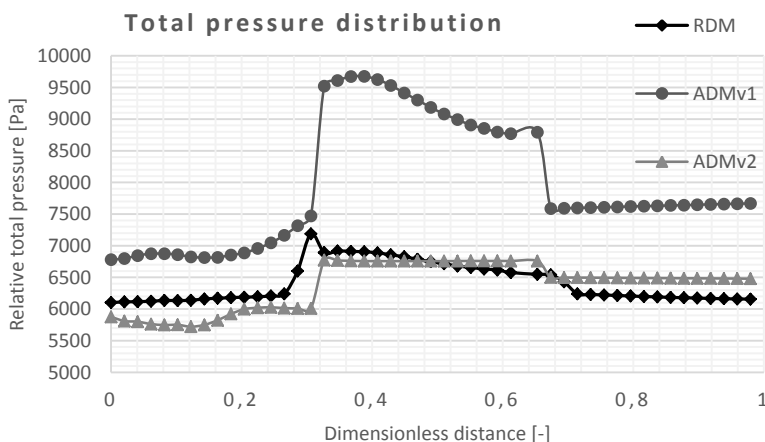

Figure 7

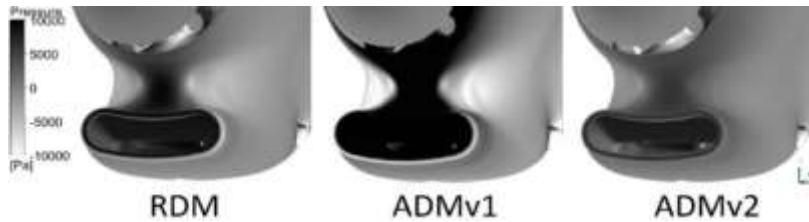Effect of the propeller on total pressure distribution

Figure 8

Relative total pressure distributions on engine nacelle downstream of the propeller blades

In order to compare the results of the different models from the propulsion viewpoint, the thrust and torque parameters of the propellers have been investigated. Each aircraft engine generates 364 kW shaft power in cruise phase, from which the generated torque is 1782.54 Nm. The thrust and torque coefficient can be calculated by the following expressions [41]:

$$c_T = \frac{T}{n^2 D^4 \rho} \text{ and } c_Q = \frac{Q}{n^2 D^5 \rho} \tag{18}$$

In equation (18) the density (ρ) was area averaged downstream of the propeller, in the same circular section. From these coefficients, the propeller efficiency in the function of J, advanced ratio, can be determined according to (19).

$$\eta = \frac{J}{2\pi}\frac{c_T}{c_q} \text{ where } J = \frac{V}{nD} \tag{19}$$

As Table 1 represents, the generated thrust forces are really close to each other in the case of the RDM and ADMv2 model, the relative difference is 1.37% between the parameters. The overestimated downstream velocity distribution by ADMv1 is resulted in 21.77% difference. Computing the area averaged density and velocity downstream of the propeller the torque, assuming that RDM is the most accurate – reference model, the thrust – torque coefficients, advanced ratios and propeller efficiencies have been calculated. The relative difference between ADMv1 and RDM were significantly high from the viewpoint of every investigated parameter, while ADMv2 provided results close to RDM, with the maximum value for the relative error of 3.92%. The propeller thrust of the ADMv1 model was not only higher but resulted in unreal propeller efficiency: 108.56%, which is not possible.

Table 1

Simulated thrust and torque parameters of the propeller

	RDM	ADMv1	ADMv2	ADMv1 rel. error [%]	ADMv2 rel. error [%]
T [N]	2968.8	3528.2	2857.6	21.77	1.37
ρ [kg/m^3]	0.8951	0.9407	0.9073	5.09	1.37
c_T [-]	0.1637	0.1897	0.1593	15.87	2.7
c_Q [-]	0.0484	0.0461	0.0478	10.58	3.92
J [-]	1.6568	1.6568	1.6568	-	-
η [-]	0.9135	1.0856	0.8793	21.77	1.37

Although for the whole geometry no experimental data is available yet, by observing the results, it can be concluded that ADMv2 model is capable of providing results close to the RDM model; so accurate results with accepted accuracy in a much shorter time can be achieved.

Conclusions

In the framework of the ESPOSA project, an aerodynamic analysis of a turboprop engine, its propeller and internal flow channels has been completed. The goal of the present work is to compare the results of different simulation approaches and develop an accurate, fast and general method for considering the effect of the propeller. Three numerical analyses have been performed and the results of the three different methods have been compared with each other are the next: Rotating Domain Model and Actuator Disk Model with two different boundary condition settings.

The computational time demand for the imbalances to reach 1% and residuum to converge untill $2*10^{-4}$ in the case of the RDM was nearly 15 days, for ADMv1 approx. 1.5 days and for ADMv2 is 0.75 day on the same computer with Intel® Core™ i7-3770 CPU and 8 GB RAM. Also, the RDM required almost 4000 iteration steps, while for ADM cases 200 iterations were sufficient. Consequently, the ADM models have significantly shorter computational time demand. According to the investigated parameters for determining the accuracy of the different approaches, the ADMv2 provides the closest results to the RDM method, which is considered to be the most accurate one due to the detailed physical and numerical representations and based on the previous validation. If the boundary conditions for the ADM (ADMv2) are the total pressure with determined flow direction and static temperature, the solver is capable of taking the effect of geometrical object downstream of the rotor blades into consideration. Hence, ADMv2 is an effective approximation and so the replacements of the Rotating Domain Model, both in terms of results and in computational time demand, are reasonable. The results could be improved by applying a finer mesh or using functional representation instead of the 10 annuli.

The investigation also supports other applications, so the developed method is intended to apply in " Small aircraft hybrid propulsion system development" supported by Hungarian national EFOP-3.6.1-16-2016-00014 project titled " Investigation and development of the disruptive technologies for e-mobility and their integration into the engineering education".

References

[1]   Rohács, D. and Rohács, J., "Magnetic Levitation Assisted Aircraft Take-Off and Landing (feasibility study – GABRIEL concept)" *Progress in Aerospace Sciences*, 85: pp. 33-50, 2016

[2]   Bera, J., and Pokorádi, L.: Monte-Carlo Simulation of Helicopter Noise, Acta Polytechnica Hungarica, 12:(2) pp. 21-32, 2015

[3]   Bréda, R., Lazar, T., Andoga, R. and Madarász L.: Robust Controller in the Structure of Lateral Control of Maneuvering Aircraft, Acta Polytechnica Hungarica, pp. 101-124, Vol. 10, No. 5, 2013

[4]   Beneda, K.: Numerical Simulation of MEMS-based Blade Load Distribution Control in Centrifugal Compressor Surge Suppression, ICNPAA 2012 Congress. American Institute of Physics, Conference Proceedings 1493, 116 (2012); http://doi.org/10.1063/1.4765479, pp. 116-123, 2012

[5]   Andoga, R., Főző, L., Madarász, L. and Karol, T.: A Digital Diagnostic System for a Small Turbojet Engine, Acta Polytechnica Hungarica, pp. 45-58, Vol. 10, No. 4, 2013

[6]   Chattopadhyay, A., and Narayan, J. R., "Optimization Procedure for Design of High-Speed Prop-Rotors" *ASCE Journal of Aerospace Engineering* Volume 7, Issue 2 (April 1994)

[7]   Cao, Y., and Yu, Z., "Numerical Simulation of Turbulent Flow around Helicopter Ducted Tail Rotor", *Aerospace Science and Technology* 9 (2005) 300-306

[8]   Fujii, K., "Progress and Future Prospects of CFD in Aerospace – Wind Tunnel and Beyond"; *Progress in Aerospace Sciences* 41 (2005) 455-470

[9]   Edwards, K. L., and Davenport C., "Materials for Rotationally Dynamic Components: Rationale for Higher Performance Rotor-Blade Design", *Materials and Design* 27 (2006) 31-35

[10]   Fu, S., and Wang, L., "RANS Modeling of High-Speed Aerodynamic Flow Transition with Consideration of Stability Theory", *Progress in Aerospace Science* 58 (2013) 36-59

[11]   Muscari R., and Mascio A. Di, "Simulation of the Viscous Flow around a Propeller using a Dynamic Overlapping Grid Approach", *First International Symposium on Marine Propulsors*, smp'09, Trondheim, Norway, June 2009

[12]   Schweighofer, J., van der Meij, K., Gronarz, A., Hargitai, Cs. L., Simongáti, Gy., Demonstration by Simulation: The Four Simulator Demonstrators of the FP7 EU Project MoVeIT!, Proceedings of Congrès SHF: Hydrodynamics and simulation applied to inland waterway and port approaches, Paris, France: Société Générale Hydrotechnique, PIANC, 2015, pp. 1-11, ISBN 979-10-93567-08-2

[13]   Huda, Z., Edi, P., Almajid, A. A., and Al-Garni, A. Z. "New Trends in Designing Markets, Configurations, and Materials for Very Light Jet Aircrafts" *ASCE Journal of Aerospace Engineering* Volume 25, Issue 3 (July 2012)

[14]   Seventh Framework Programme, Theme [AAT.2011.4.4-4.], Project ESPOSA: Annex I – "Description of Work", Grant agreement no: 284859, Version date: 2011-09-20

[15]   Rácz, N., Kristóf, G., Weidinger, T.: Evaluation and Validation of a CFD Solver Adapted to Atmospheric Flows: Simulation of Topography-induced Waves, "Időjárás" / Quarterly Journal of the Hungarian Meteorological Service, 117:(3) pp. 239-275, 2013

[16]   Wald, Q. R., "The Aerodynamics of Propellers"; *Progress in Aerospace Sciences* 42, pp. 85-128, 2006

[17]   Jeromin, A., Bentamy, A., and Schaffarczyk, A. P., "Actuator Disk Modeling of the Mexico Rotor with OpenFOAM"; *ITM Web of Conferences 2*. 06001, DOI: 10.1051/itmconf/20140206001, 2014

[18]   Rankine, W. J. M., "On the Mechanical Principles of the Action of Propellers". *Transactions Institute of Naval Architects 6*, p. 13, 1865

[19]   Froude, R. E., "On the Part Played in Propulsion by Differences of Fluid Pressure". *Transactions of the Institute of Naval Architects 30,* pp. 390-405, 1889

[20]   Glauert H., "Airplane Propellers". *Aerodynamic theory. Ed. by W. F. Durand. Vol. IV*, Division L. Springer, 1935, pp. 169-360

[21]   Wu, T. Y., "Flow through a Heavily Loaded Actuator Disc". *Schiffstechnik 9* (1962) pp. 134-138

[22]   Conway J. T., "Exact Actuator Disk Solutions for Non-Uniform Heavy Loading and Slipstream Contraction". *J. Fluid Mech.* 365 (1998) pp. 235-267

[23]   Bontempo, R., Manna, M., "Solution of the Flow over a Non-Uniform Heavily Loaded Ducted Actuator Disk". *Journal of Fluid Mechanics* 728 (2013) pp. 163-195. ISSN: 1469-7645

[24]   Bontempo, R., Manna, M., "A Nonlinear and Semi-Analytical Actuator Disk Method Accounting for General Hub Shapes: Part I - Open Rotor". *Journal of Fluid Mechanics* (2016) DOI: 10.1017/jfm.2016.98

[25]   Costa Gomes, V. M. M. G., Palma, J. M. L. M., and Silva Lopes, A., "Improving Actuator Disk Wake Model", *Journal of Physics: Conference Series* 524 (2014) 012170, TORQUE 2014

[26]   Gravdahl, A. R., Crasto, G., Castellani, F., and Piccioni E., "Wake Modeling with the Actuator Disc concept", *Energy Procedia 24* (2012) 385-392

[27]   Yu, N. J., Samant, S. S., Rubbert, P. E., "Flow Prediction for Propfan Configurations using Euler Equations", *AIAA 84-1645, 17th Fluid Dynamics, Plasma Dynamics and Lasers Conference*, June 1984, Snowmass, Colorado

[28]   Le Chuiton, F., "Actuator Disc Modeling for Helicopter Rotors", *Aerospace Science and Technology* Volume 8, Issue 4 2004, pp. 285-297

[29] Visingardi, A., Khier, W., and Decours, J., "The Blind-Test Activity of Tiltaero Project for the Numerical Aerodynamic Investigation of a Tilt Rotor", *ECOMAS 2004* Jyväskylä, 24-28 July 2004

[30] Conlisk, A. T., "Modern Helicopter Rotor Aerodynamics"; *Progress in Aerospace Sciences*, 37 (2001) 419-476

[31] Farrokhfal, H., and Pishevar, A. R., "Aerodynamic Shape Optimization of Hovering Rotor Blades using a Coupled Free Wake-CFD and Adjoint Method", *Aerospace Science and Technology* 28 (2013) 21-30

[32] Lenfers, C., "Propeller Design for future QESTOL Aircraft in the BNF Project", *30th AIAA Applied Aerodynamics Conference* 25-28 June 2012, New Orleans, Louisiana; AIAA 2012-3334

[33] Coton, F. N., Marshall, J.S., Galbraith, R. A. Mc D., Green, R. B., "Helicopter Tail Rotor Orthogonal Blade Vortex Interaction", *Progress in Aerospace Sciences* 40 (2004) 453-486

[34] Blazek, J., "*Computational Fluid Dynamics: Principle and Applications*", Elsevier, ISBN-13: 978-0-08-044506-9, ISBN-10: 0-08-044506-3, United Kingdom, 2005

[35] ANSYS, Inc., "ANSYS CFX-Solver Theory Guide", Release 12.0, ANSYS, Inc. Southpointe, 275 Technology Derive Canonsburg, PA 15317, ansysinfo@ansys.com, http://www.ansys.com, USA, April 2009

[36] Gausz, T., "Légcsavarok", Electronic Lecture Notes, Budapest, 31.01.2015., http://www.ara.bme.hu/oktatas/tantargy/NEPTUN/BMEGEATAKV4/ 2015-2016-I /ea/LEGCSAVAROK.pdf, 21.06.2015

[37] VZLU, ESPOSA Project, "WP6.2.4. BE2 Tractor Configuration: Propeller Characteristics", *Workshop Presentation*, 05.2015

[38] International Organization for Standardization, Standard Atmosphere, ISO

[38] 2533:1975, 1975

[39] Amato, M., Boyle, F., Eaton, J. A., and Gardarein, P., "Euler/Navier-Stokes Simulation for Propulsion-Airframe Integration of Advanced Propeller-Driven Aircraft in the European Research Programs GEMINI/APIAN"; *21st ICAS Congress* 13-18/09/1998, ICAS-98-5,10,2, Australia

[40] EVEKTOR, "Specification of Engine and Airframe Installation Requirements of ACC TR2", NO. ACP1-GA-2011-284859-ESPOSA

[41] Rwigema, M. K., "Propeller Blade Element Momentum Theory with Vortex Wake Deflection", *27th Congress of International Council of the Aeronautical Sciences* (2010) 19-24 September 2010, Nice, France Paper ICAS 2010-2.3.3

[42] Renaud, T., O'Brien, D., Smith, M., Potsdam, M., "Evaluation of Isolated Fuselage and Rotor-Fuselage Interaction using CFD", *American Helicopter Society 60th Forum*, Baltimore, MD, June 7-10, 2004